Lattice Monte Carlo study of orientational order in a confined system of biaxial particles: Effect of an external electric field

João Paulo Casquilho [1] and João Luis Figueirinhas [2,*]

[1] *LIBPhys-UNL-Laboratory for Instrumentation, Biomedical Engineering and Radiation Physics, Department of Physics, NOVA School of Science and Technology, NOVA University Lisbon, Largo da Torre, 2825-149 Caparica, Portugal*

[2] *Centre for Physics and Engineering of Advanced Materials and Physics Department, Instituto Superior Técnico, Universidade de Lisboa, Avenida Rovisco Pais,1, 1049-001 Lisbon, Portugal*

(Received 5 November 2020; accepted 17 February 2021; published 15 March 2021)

In this work we have used lattice Monte Carlo to determine the orientational order of a system of biaxial particles confined between two walls inducing perfect order and subjected to an electric field perpendicular to the walls. The particles are set to interact with their nearest neighbors through a biaxial version of the Lebwohl-Lasher potential. A particular set of values for the molecular reduced polarizabilities defining the potential used was considered; the Metropolis sampling algorithm was used in the Monte Carlo simulations. The relevant order parameters were determined in the middle plane of the sample and for some cases across the whole thickness of the sample. We have determined the temperature–electric field phase diagram for this system and found, as expected, five different system configurations corresponding to three different mesophases. At low temperatures and low fields the system finds itself in an undistorted biaxial phase. On increasing the field at low temperatures, a Freedericksz transition takes place and the secondary directors reorient towards the field while the primary director stays undistorted and parallel to the walls. On increasing the field further, a second Freedericksz transition occurs and the primary director orients also towards the field direction. The orientational order measured at the field strengths tested is not affected by the field. On increasing the temperature, a transition to a uniaxial phase occurs and within the range of this phase a field increase leads also to a Freedericksz transition where the main director reorients towards the field. At higher temperature a transition to a disordered phase is found. We have performed finite size scaling analysis for the Freedericksz critical fields and found that they scale with the distance L between the walls as L^{-1} as expected from continuum theory. From these fields we have also determined the temperature dependence of two elastic constant ratios. Critical exponents and critical temperatures for the order parameter and the correlation length for the biaxial-uniaxial phase transition and the uniaxial to disordered phase transition were also determined by finite size scaling and are discussed.

DOI: 10.1103/PhysRevE.103.032701

I. INTRODUCTION

Biaxial nematics have attracted significant attention from liquid crystal researchers since the 1970s; the seminal works of Freiser [1], Alben [2], and Straley [3] paved the way for a large body of both theoretical and experimental studies dedicated to this subject. Considered by many as one of the important problems in liquid crystal physics [4], it is one more case where experimental evidence [5] lagged behind theoretical predictions [1]. One of the techniques that allowed significant progress in this area is Monte Carlo simulations that were used early in studying this problem [6] and have been explored quite extensively ever since [7]. The experimental evidence for the spontaneous formation of a macroscopic thermotropic biaxial nematic monodomain, as proposed by Freiser [1], has been lacking in low molecular weight liquid crystals [4]. The known results are consistent with the macroscopic ordering of local biaxial domains under the effect of directional surface anchoring or applied aligning fields, which led to the development of the cluster model of biaxial nematics. The basic assumption of this model is a nematic phase consisting of biaxial microdomains which, in the absence of external stimulus, are randomly distributed into a macroscopically uniaxial nematic state [8].

The response of a bulk biaxial nematic to an applied external field has been studied by several authors [9–11]. In Ref. [11] virtual molecular dynamics computer experiments on biaxial Gay-Berne particles were analyzed and it was found that switching of the secondary directors is up to an order of magnitude faster than that of the main director. This fact indicates that the biaxial elastic constants are expected to be significantly weaker than the uniaxial ones.

Capacitance measurements were performed on an organosiloxane tetrapode material as a function of the applied AC voltage, exhibiting a biaxial nematic phase [12]. For a planar sample, in the uniaxial nematic (N_U) temperature range, the Freedericksz transition occurs and the capacitance starts to rise as V increases from the critical value, as the director aligns with the applied field. In the biaxial nematic (N_B) phase it could be expected that beyond the field induced reorientation of the primary director, a reorientation of the

*Corresponding author: joao.figueirinhas@tecnico.ulisboa.pt

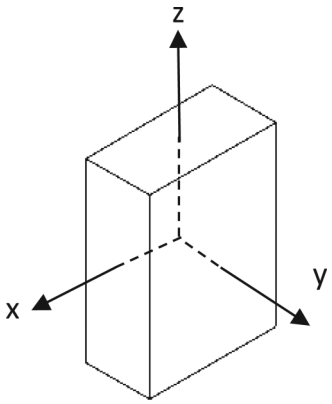

FIG. 1. Biaxial molecules with orthorhombic symmetry are considered; x, y, z: molecular principal axis.

secondary directors would occur. This occurrence was not experimentally observed, although the secondary directors could, in principle, reorient at either a much lower or much higher threshold voltage than the primary director, and in this way escape direct observation in the work by Polineni *et al.* [12].

In this work, a sample geometry where the long axis and the face of the molecules are anchored parallel to the wall and the field is applied perpendicular to the wall is considered for the Monte Carlo simulations. The MC simulations are carried out using a biaxial version of the Lebwohl-Lasher potential [13,14] with a particular set of values for the reduced molecular polarizabilities defining the potential [15]. For several values of the thickness of the cell, (1) we study the transition from the surface aligned to the field aligned state of both the principal and the secondary axes, and obtain the correspondent Freedericksz critical fields; (2) we obtain the critical temperatures and critical exponents of the uniaxial and (the more relevant) biaxial order parameters, for a (weaker than the critical) value of the applied field. The characterization of the system is necessary in order to determine the biaxial and the uniaxial range, in the first place. It is shown that at low temperatures a biaxial phase and a subsequent uniaxial phase are present and the field effect simulations can thus be performed.

II. SINGLE SITE LATTICE MODEL

The liquid crystal is described by a collection of fixed interacting sites on a three-dimensional (3D) lattice, with orientational degrees of freedom. The interacting sites may represent a single molecule or a uniformly oriented microdomain with orthorhombic symmetry, in the context of the cluster model [8]. See Fig. 1.

The working lattice dimensions are $d \times L \times d$ sites, with $L = 10$, 20, 30, 40, and 60. The L dimension gives the thickness of the cell, upon which are imposed rigid boundary conditions corresponding to planar alignment of the uniaxial director and with the faces of the molecules parallel to the wall. On the two other directions periodic boundary conditions are imposed. Values $d = 6$, 8, 10, 12, 14, 16, and 18, were used, which allows a finite size scaling analysis to study the thickness dependence of the Freedericksz critical fields and of the critical temperatures and exponents of the relevant order parameters, in both the biaxial and the uniaxial phases.

III. BIAXIAL SYSTEM AND INTERACTION POTENTIAL

The pair potential is a biaxial generalization to D_{2h} symmetry of the Lebwohl-Lasher potential [14] used by several authors to study liquid crystal (LC) systems of biaxial molecules [16–18] in Cartesian form [16]; it reads

$$U = -\varepsilon[(3V_{33} - 1)/2 - \lambda\sqrt{6}(V_{11} - V_{22}) + \lambda^2(V_{11} + V_{22} - V_{12} - V_{21})], \quad (1)$$

where $V_{ij} = (\boldsymbol{u}_i \cdot \boldsymbol{v}_j)^2$ and $\boldsymbol{u}_i, \boldsymbol{v}_j$, $i, j = 1, 2, 3$, are the three axes of the two interacting molecules. As shown in Refs. [19,20], U is made up of couplings between the principal axes of neighboring molecules, and constitutes a particular case of the more general potential studied there. ε is an interacting energy between neighboring particles and λ is a parameter depending on molecular properties. In the case of dispersive interactions, and considering mesogens as rigid boardlike particles, the parameter λ can be expressed in terms of the diagonal elements of the reduced polarizability tensor $\boldsymbol{\alpha}$ of the molecule [16]:

$$\lambda = \sqrt{\frac{3}{2}}\frac{\alpha_{xx} - \alpha_{yy}}{2\alpha_{zz} - (\alpha_{xx} + \alpha_{yy})}. \quad (2)$$

The reduced energy U/ε is used in the simulations. $\lambda = 0$ corresponds to the uniaxial system. The value $\lambda = 1/\sqrt{6} \cong 0.408$ characterizes the change from prolate to oblate molecules. The following reduced polarizabilities, defined relatively to the principal molecular axes [15], are used in the simulations with the applied field: $\alpha_{zz} = 0.6$, $\alpha_{xx} = 0.3$, and $\alpha_{yy} = 0.1$, which give $\lambda \cong 0.306$, in the prolate region. The choice of these values for the reduced polarizabilities was motivated by their use in the mean field theory study reported in Ref. [15]. Their study indicates that, in the prolate uniaxial nematic N_U phase, the axis associated with the largest polarizability tends to align in a preferred direction, while the minor axes associated with the smaller polarizabilities are randomly distributed in a plane which is orthogonal to the preferred direction of the largest axis. In contrast, in the biaxial N_B phase the minor axes show strong biaxiality ([15], p. 484).

IV. ORDER PARAMETERS

In this section we outline the calculation of the order parameters necessary to describe uniaxial and biaxial ordering. For a rigid molecule or molecular segment this can be achieved by the ordering matrix [21],

$$S^{ij}_{\alpha\beta} = \left\langle \tfrac{3}{2}\cos(\theta_{i\alpha})\cos(\theta_{j\beta}) - \tfrac{1}{2}\delta_{ij}\delta_{\alpha\beta} \right\rangle, \quad (3)$$

where $\langle\rangle$ denotes an ensemble average and $\theta_{i\alpha}$ is the angle between the i axis of the laboratory axes frame and the α axis of the rigid molecule or molecular segment axes frame. δ_{ij} is the Kronecker symbol. For a rigid molecule or molecular segment with D_{2h} symmetry and limiting the characterizable systems to those with D_{2h} symmetry or higher, the relevant order parameters can be reduced to four by a proper choice of

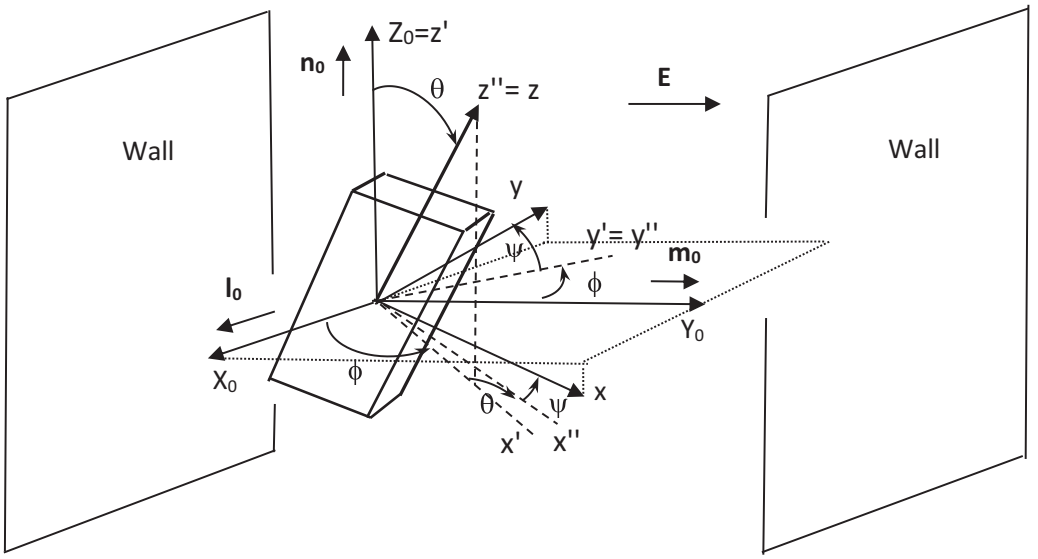

FIG. 2. Geometry of the sample.

both the molecule and the laboratory axes frames [21].

$$S \equiv S_{zz}^{ZZ}, \tag{4a}$$

$$P \equiv S_{zz}^{XX} - S_{zz}^{YY}, \tag{4b}$$

$$D \equiv S_{xx}^{ZZ} - S_{yy}^{ZZ}, \tag{4c}$$

$$C \equiv S_{xx}^{XX} - S_{yy}^{XX} - S_{xx}^{YY} + S_{yy}^{YY}. \tag{4d}$$

S gives the degree of uniaxial order and C is a measure of intrinsic biaxiality and is the most appropriate quantity to identify the biaxial phase. P is a phase biaxiality parameter and D is a molecular asymmetry parameter [21].

The appropriate reference frames involved in the determination of the four order parameters S, D, P, and C include the molecular frame x, y, z and the laboratory frame X, Y, Z. The x, y, z molecular frame has its axes coinciding with the symmetry axes of the D_{2h} symmetric molecule and was defined as the eigenframe of the molecular polarizability tensor. Regarding the X, Y, Z laboratory frame, the Z axis is determined as the axis parallel to the eigenvector $\widehat{u_Z}$, of the Saupe tensor S_{zz}^{ij} associated with the largest eigenvalue. The tensor S_{xx}^{ij} was also diagonalized and the eigenvector $\widehat{u_{X'}}$, associated with its largest eigenvalue modulus, was used to define the Y axis through the relation $\widehat{u_Y} = \frac{\widehat{u_Z} \times \widehat{u_{X'}}}{|\widehat{u_Z} \times \widehat{u_{X'}}|}$. The tensors S_{zz}^{ij} and S_{xx}^{ij} are calculated at the end of each Monte Carlo cycle for the different L layers in the sample, using the laboratory fixed reference frame (X_0, Y_0, Z_0). The order parameters S, D, P, and C can be cast in terms of the Euler angles ϕ, θ, Ψ defining the spatial orientation of the molecular x, y, z frame in the X, Y, Z laboratory frame.

At the walls, the long axis of the molecule points in the Z_0 direction and the face is parallel to the wall. $\mathbf{n}_0$, $\mathbf{l}_0$, and $\mathbf{m}_0$ are the triplet of directors, corresponding to D_{2h} symmetry, at the walls and uniformly across the sample at the initial configuration.

In the convention described in Fig. 2 [22], the order parameters can be written as [17]

$$S \equiv S_{zz}^{ZZ} = \left\langle R_{0,0}^2 \right\rangle = \tfrac{1}{2}\langle 3\cos^2\theta - 1\rangle, \quad -\tfrac{1}{2} \leqslant S \leqslant 1, \tag{5a}$$

$$P \equiv S_{zz}^{XX} - S_{zz}^{YY} = \sqrt{6}\left\langle R_{2,0}^2 \right\rangle = \tfrac{3}{2}\langle \sin^2\theta \cos 2\phi\rangle, \tag{5b}$$

$$D \equiv S_{xx}^{ZZ} - S_{yy}^{ZZ} = \sqrt{6}\left\langle R_{0,2}^2 \right\rangle = \tfrac{3}{2}\langle \sin^2\theta \cos 2\psi\rangle, \tag{5c}$$

$$C \equiv S_{xx}^{XX} - S_{yy}^{XX} - S_{xx}^{YY} + S_{yy}^{YY} = 6\left\langle R_{2,2}^2 \right\rangle$$
$$= 3\left\langle \tfrac{1}{2}(\cos^2\theta + 1)\cos 2\phi \cos 2\psi \right.$$
$$\left. -\cos\theta \sin 2\phi \sin 2\psi \right\rangle, \quad -3 \leqslant C \leqslant 3, \tag{5d}$$

where $\langle\rangle$ denotes an ensemble average.

In a Monte Carlo cycle (MCC), i.e., one run over the lattice, in each step on consecutive sites one of the Euler angles is randomly chosen with a value between 0° and 360°, also randomly chosen. This move is accepted or not according to the Metropolis method [23]. For the calculation of the relevant quantities, the Metropolis sampling algorithm is used. Two million MCCs were used for equilibration and subsequently the averages were calculated over 1 000 000 MCCs.

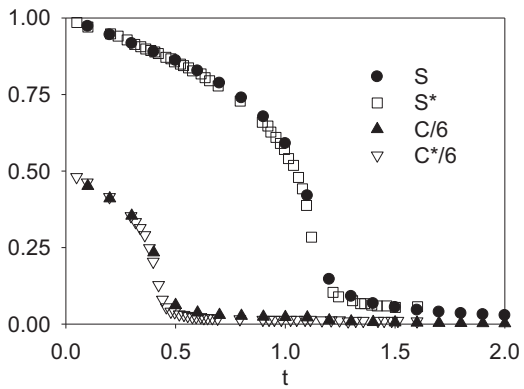

FIG. 3. Comparison between the temperature dependencies of the order parameters S and C for our y-bounded samples (filled circles and triangles) with $\lambda = 0.306$, $L = n_y = 30$, $n_x = n_z = 10$, determined halfway between the y bounds and the S and C values (marked with *) for unbounded samples, with $\lambda = 0.3$ and $n_x = n_y = n_z = 10$ [17].

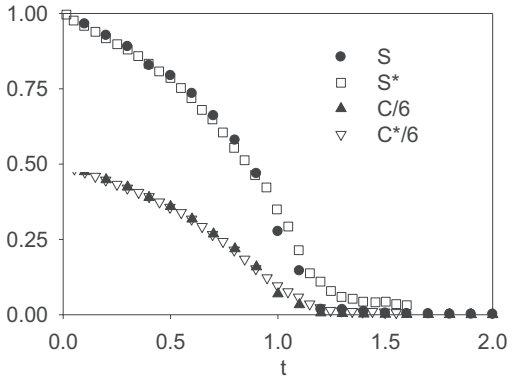

FIG. 4. Comparison between the temperature dependencies of the order parameters S and C for our y-bounded samples (filled symbols) with $\lambda = 0.4$, $L = n_y = 40$, $n_x = n_z = 10$, determined halfway between the walls and the S and C values (marked with *) for unbounded samples with $\lambda = 0.408$ and $n_x = n_y = n_z = 10$ [17].

V. THERMAL CHARACTERIZATION OF THE SYSTEM

The simulations are started with a uniformly oriented sample, where the molecules are ordered like books in a bookcase, with strong anchoring at the walls. Our results for the order parameters are consistent with the ones obtained from calculations with respect to the instantaneous orientation in unbounded samples [17,24] and references therein as shown in Figs. 3 and 4. At low temperatures, a *biaxial nematic phase* (N_B) shows up, where the molecules or the clusters align not only their major axes but also their faces. At higher temperatures, the plot of the order parameters as a function of the reduced temperature $t = k_BT/\varepsilon$ shows two temperature driven phase transitions: *a biaxial-uniaxial transition to a uniaxial nematic phase* (N_U) and a *uniaxial-isotropic transition to an isotropic phase (I)*. These figures are shown just for the sake of comparison with published results. In what follows we will systematically study the critical temperatures for our systems.

VI. EFFECT OF AN APPLIED ELECTRIC FIELD

The goal is to calculate the effect of an applied electric field normal to the boundaries (a) on the director deviations

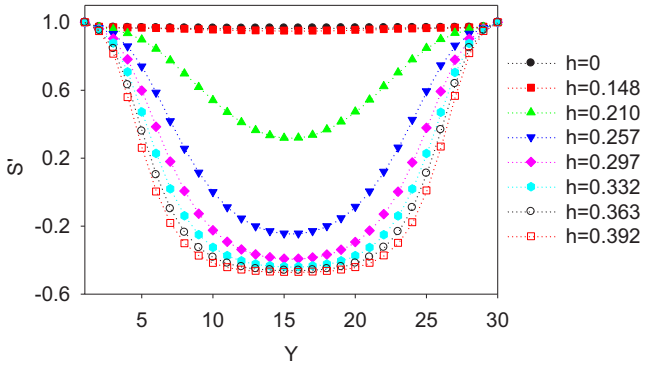

FIG. 5. Y dependence values for the order parameter S' for $t = 0.1$ and different fields with strengths indicated, going above the Freedericksz transition field for the main director. $n_x = n_z = 10$, $L = n_y = 30$.

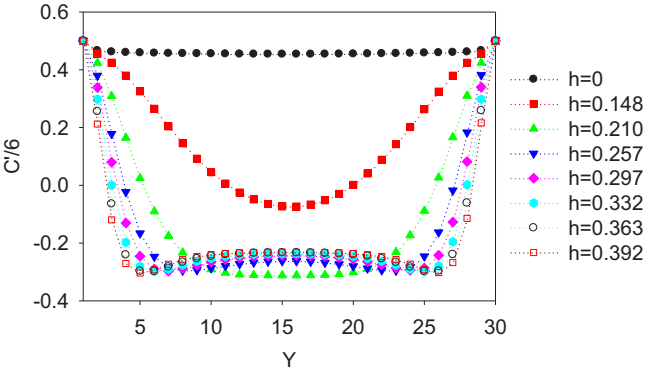

FIG. 6. Y dependence of the apparent values for the order parameter $C'/6$ for $t = 0.1$ and different fields strengths as indicated. $n_x = n_z = 10$ and $L = n_y = 30$.

from the boundary imposed orientation and (b) its effect on the intrinsic nematic order.

The interaction energy of a single molecule with the applied field is given by

$$U = \xi\, E^2 \sum_i \varepsilon_i, \tag{6}$$

where ξ determines the sign and the strength of coupling with the electric field E, and

$$\varepsilon_i = -\alpha_{ii}\tfrac{1}{2}[3(\boldsymbol{u_i}\cdot\boldsymbol{e})^2 - 1], \quad i = x, y, z, \tag{7}$$

where the α_{ii} are the reduced polarizabilities, defined above, such that $\sum_i \alpha_{ii} = 1$, the $\boldsymbol{u}_i$ are the three axes of the molecule, and $\boldsymbol{e}$ is the direction of the applied field [15].

As in the calculations of the reduced anisotropic pair interaction, the energy U/ε is used; the parameter entering the simulations for the energy associated with the (local) field strength acting on each site is $h^2 \equiv \xi E^2/\varepsilon$. In the following, we study both the effect, measured by the order parameters, of the variation of the average orientation of the molecules with respect to the anchoring walls and of the variation of the intrinsic order (uniaxial or biaxial) with the applied field (see Discussion). The results were obtained with the values of the reduced polarizabilities given above.

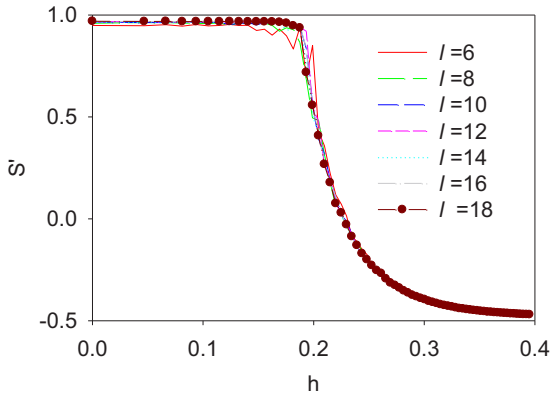

FIG. 7. Field dependence of the apparent order parameter S' determined halfway between the sample walls for $t = 0.1$, $n_y = 30$ and different values of $l = n_x = n_z$ ranging from 6 to 18.

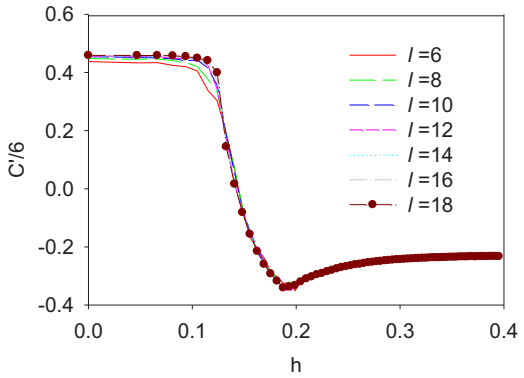

FIG. 8. Field dependence of the apparent order parameter $C'/6$ determined halfway between the sample walls for $t = 0.1$, $n_y = 30$ and different values of $l = n_x = n_z$ ranging from 6 to 18.

Order parameters

Figures 5 and 6 report the y dependence of the apparent values for the order parameters S and $C/6$, named, respectively, as S' and $C'/6$ (as the values obtained for S and C are not their true values because their expressions were evaluated considering the laboratory frame X_0, Y_0, Z_0 and not the X, Y, Z frame indicated above) within the sample for different fields within the N_B phase with $t = 0.1$. Figures 7 and 8 report the electrical field dependence of the apparent values for the order parameters S' and $C'/6$ determined halfway between the sample walls within the N_B phase for $t = 0.1$, $n_y = 30$, and different values of $l = n_x = n_z$ ranging from 6 to 18. The Freedericksz transitions corresponding to the reorientation of the primary and secondary directors n and m, l, respectively, are clearly evidenced by the field dependence of the apparent values of the order parameters S' and $C'/6$, respectively. The successive reorientation of the secondary (m, l) and primary (n) directors as the applied field grows is schematically depicted in Fig. 9.

The behavior of the order parameters' field susceptibilities as a function of the applied field is a good indicator of the onset of a phase transition. Here the interesting ones are the S and C susceptibilities. These quantities are calculated from the fluctuation-dissipation relations $\chi_S = N(\langle S^2\rangle - \langle S\rangle^2)/(k_B T)$ and $\chi_C = N(\langle C^2\rangle - \langle C\rangle^2)/(k_B T)$, reduced by the sample size, which allows direct comparison for different sample sizes or the derivatives of the order parameters with respect to the field and are reported in Figs. 10 and 11.

Figures 12–15 report a systematic determination of the reduced temperature dependence of the order parameters S and C and also their apparent values for $h = 0$.

VII. SYSTEM PHASE DIAGRAM

A phase diagram for the system was determined in the t-h plane and is shown in Fig. 16. Five system configurations and three phases are detected as expected. The transition lines were determined from the peak positions of the order parameter temperature and field susceptibilities. The transition lines are all continuous in this case due to the y confinement of the system and the limited $n_x = n_z$ size. The N_B-N_U phase transition temperature shows an increase of 4.7% in the field range of $h = 0.1$ to 0.2 while the N_U-I (isotropic) phase transition temperature shows a steady increase dt/dh of 0.37 for h in the interval 0.15–0.3. The Freedericksz critical fields for the N_{B1}-N_{B2} and N_{B2}-N_{B3} transitions, respectively, E_{1c} and E_{2c}, show relatively steady values over the majority of the N_B range and their ratio $E_{2c}/E_{1c} = h_{2c}/h_{1c}$ varies between 1.43 and 1.74. Regarding the experimental accessibility of these fields, the field E_{2c} was easily reached in a tetrapode system reported in Ref. [12] by Polineni *et al.* but as discussed before E_{1c} could not be experimentally detected in that work.

VIII. FREEDERICKSZ CRITICAL FIELDS AND ELASTIC CONSTANTS

The Freedericksz transition fields shown in the systems' phase diagram (see Fig. 16) can be used to determine relations between the elastic constants and the electric permittivities as defined in the continuous description of field induced nematic distortions [25].

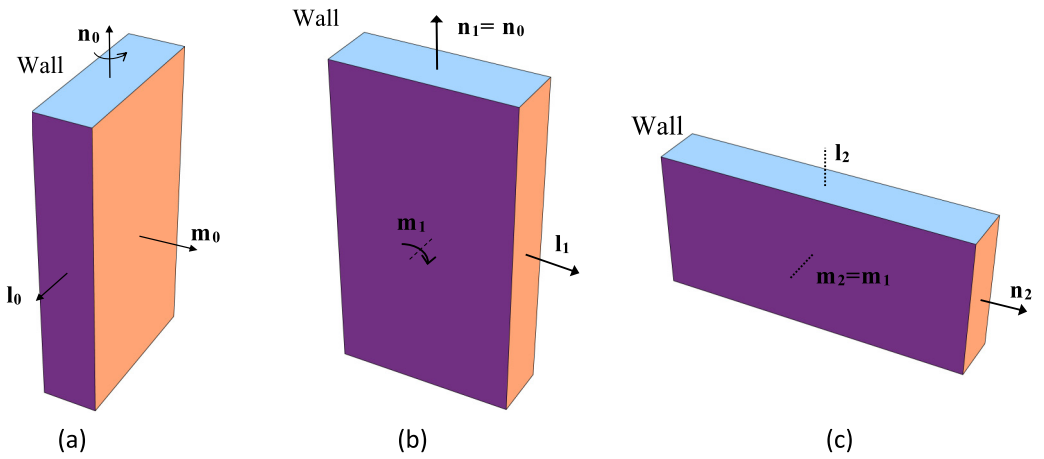

FIG. 9. Case (a) reports the initial director configuration, as in Fig. 2. [$S' = 1$, $C'/6 = 1/2$ (athermal)]. Case (b) shows the directors configuration after a 90° rotation around $\mathbf{n}_0$ ($S' = 1$, $C'/6 = -(1/2)$ (athermal)]. Case (c) reports the director configuration after a second 90° rotation around $\mathbf{m}_1$ [$S' = -(1/2)$, $C'/6 = -(1/4)$ (athermal).

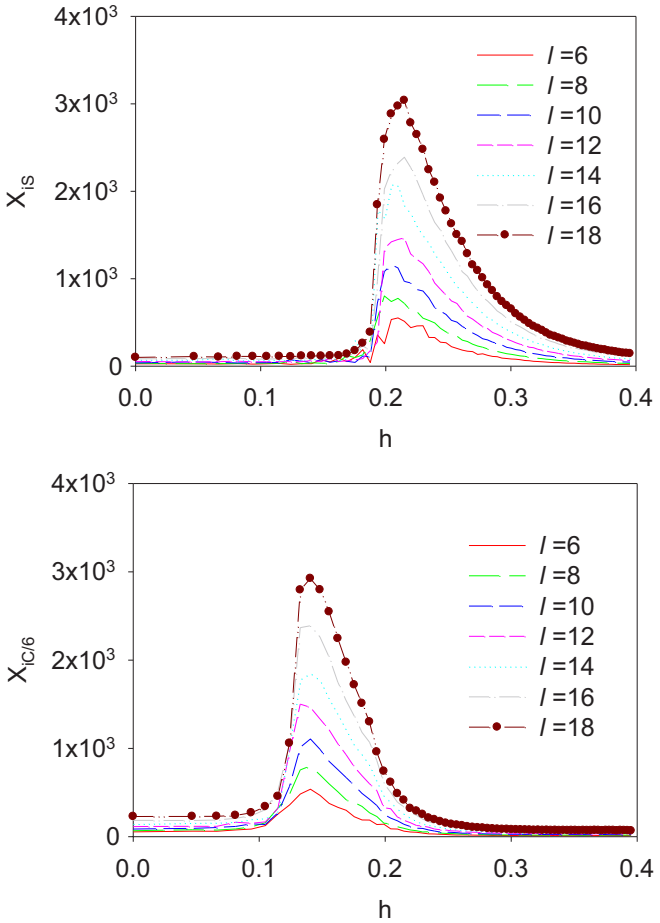

FIG. 10. Order parameters' susceptibilities as a function of applied field obtained from the fluctuation-dissipation relation, for the apparent order parameters S' and $C'/6$ reported in Figs. 7 and 8.

Considering the elastic free energy density for the biaxial nematic phase proposed by Trebin [26] along with the simplifying assumptions listed below and the nematic directors **n**, **m**, and **l** parallel, respectively, to the Z, Y, X axes of the laboratory frame expressed in terms of the Euler angles α, β, and δ, one obtains for the elastic contribution to the free energy density of the nematic the expression

$$
\begin{aligned}
2F_k = &\left\{k_{n1}\cos(\alpha)^2\sin(\beta)^2 + \frac{1}{4}k_{n2}\sin(\alpha)^2\sin(2\beta)^2\right.\\
&+ k_{n3}\left[\sin(\beta)^2 - \cos(\alpha)^2 - \frac{1}{4}\sin(\alpha)^2\sin(2\beta)^2\right]\\
&\left.+ k_m(1+\cos(\beta)^2)\right\}\left(\frac{\partial\alpha}{\partial y}\right)^2 + \frac{1}{2}(k_{n1}-k_{n2})\\
&\times \sin(2\alpha)\sin(2\beta)\left(\frac{\partial\alpha}{\partial y}\right)\left(\frac{\partial\beta}{\partial y}\right) + \{k_{n1}\sin(\alpha)^2\cos(\beta)^2\\
&+ k_{n2}\cos(\alpha)^2 + k_{n3}\sin(\alpha)^2\sin(\beta)^2 + k_m\}\left(\frac{\partial\beta}{\partial y}\right)^2\\
&+ 2k_m\cos(\beta)\left(\frac{\partial\alpha}{\partial y}\right)\left(\frac{\partial\delta}{\partial y}\right) + k_m\left(\frac{\partial\delta}{\partial y}\right)^2 \qquad (8)
\end{aligned}
$$

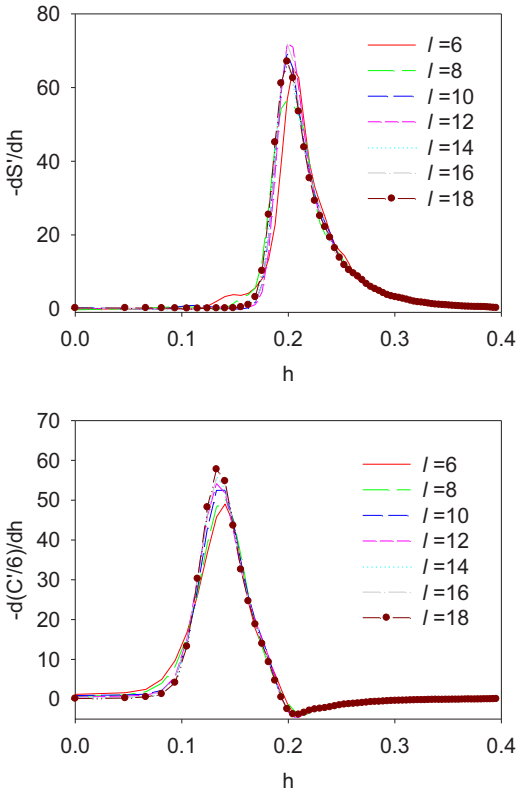

FIG. 11. Order parameters' susceptibilities as a function of applied field obtained from $-dS'/dh$, $-d(C'/6)/dh$, for the apparent order parameters S' and $C'/6$ reported in Figs. 7 and 8.

Expression (8) stems from Ref. [26] when the elastic constants for the secondary directors are all assumed identical to k_m and the cross terms between different directors are neglected; also the Euler angles α, β, and δ are assumed to be solely dependent upon the y coordinate which runs normal to the boundary plates. The contribution to the free energy from the interaction with the electrical field takes

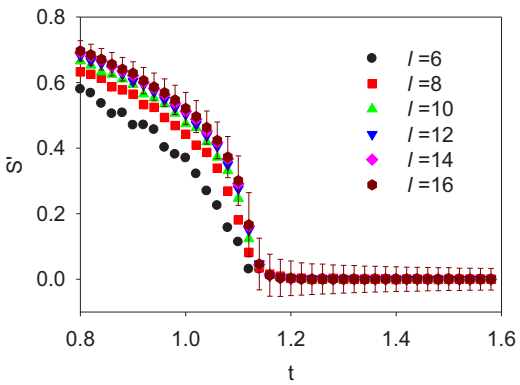

FIG. 12. Reduced temperature dependence of the apparent order parameter S' determined halfway between the sample walls for $n_y = 30$ and different values of $l = n_x = n_z$ ranging from 6 to 16 and $h = 0$. The error bars indicate the standard deviation of the reported values.

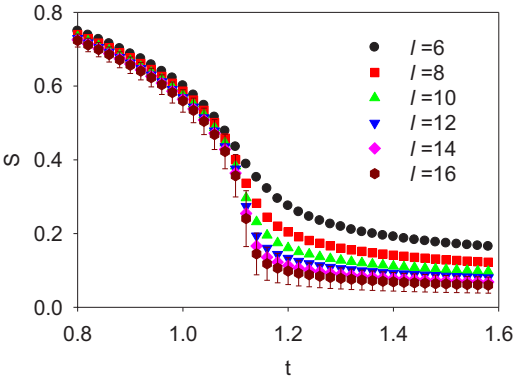

FIG. 13. Reduced temperature dependence of the order parameter S determined halfway between the sample walls for $n_y = 30$ and different values of $l = n_x = n_z$ ranging from 6 to 16 and $h = 0$. The error bars indicate the standard deviation of the reported values.

the form

$$2F_E = -E_y^2\{\varepsilon_{nn}n_y^2 + \varepsilon_{mm}m_y^2 + \varepsilon_{ll}l_y^2\}, \tag{9}$$

where ε_{ii} are the electrical permittivities.

The total free energy density $F_K + F_E$ along with the geometry of the problem lead to the existence of two Freedericksz transition fields E_{1c} and E_{2c} given by

$$E_{1c} = \frac{\pi}{L}\sqrt{\frac{2k_m}{\varepsilon_{ll} - \varepsilon_{mm}}} = h_{1c}\left(\frac{\varepsilon}{\xi}\right)^{1/2},$$
$$E_{2c} = \frac{\pi}{L}\sqrt{\frac{k_{n1} + k_m}{\varepsilon_{nn} - \varepsilon_{mm}}} = h_{2c}\left(\frac{\varepsilon}{\xi}\right)^{1/2}. \tag{10}$$

E_{1c} corresponds to the onset field for a distortion involving exclusively a reorientation of the secondary directors **l** and **m** and E_{2c} corresponds to the onset field for a distortion involving the reorientation of the primary director **n**. Combining the expressions in Eq. (10) with the known relations for the permittivity tensor components [27] one obtains for the ratio

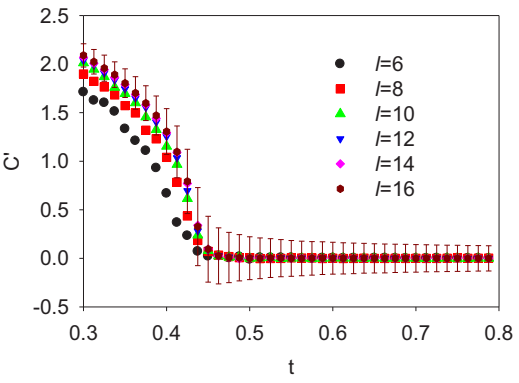

FIG. 14. Reduced temperature dependence of the apparent order parameter C' determined halfway between the sample walls for $n_y = 30$ and different values of $l = n_x = n_z$ ranging from 6 to 16 and $h = 0$. The error bars indicate the standard deviation of the reported values.

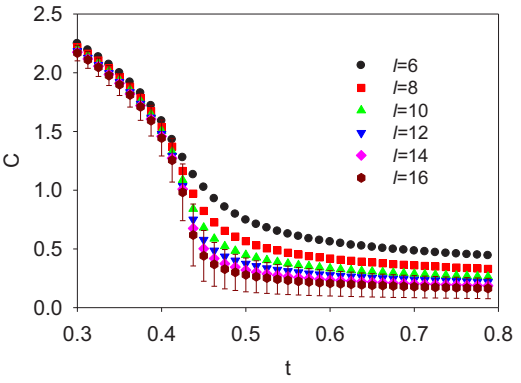

FIG. 15. Reduced temperature dependence of the order parameter C determined halfway between the sample walls for $n_y = 30$ and different values of $l = n_x = n_z$ ranging from 6 to 16 and $h = 0$. The error bars indicate the standard deviation of the reported values.

of elastic constants k_m/k_{n1} and the reduced elastic constants sum $(k_{n1} + k_m)/k_a$ the following expressions:

$$\frac{k_m}{k_{n1}} = \left[2\left(\frac{h_{2c}}{h_{1c}}\right)^2 \frac{\alpha_1(S+P/3)+\alpha_2(D/2+C/6)}{2\alpha_1 P/3+\alpha_2 C/3} - 1\right]^{-1},$$
$$\frac{k_{n1} + k_m}{k_a} = h_{2c}^2\,[\alpha_1(S + P/3) + \alpha_2(D/2 + C/6)], \tag{11}$$

where $\alpha_1 \equiv \alpha_{nn} - (\alpha_{ll} + \alpha_{mm})/2$, $\alpha_2 \equiv \alpha_{ll} - \alpha_{mm}$, and $k_a \equiv 3(\frac{L}{\pi})^2 \frac{\varepsilon}{\xi}\bar{\chi}$. $\bar{\chi}$ is the isotropic part of the electric susceptibility tensor. The relations in Eq. (11) are graphed in Fig. 17 for the temperature range 0.1–0.4. with $n_y = 30$ and $n_x = n_z = 16$.

IX. FINITE SIZE SCALING ANALYSIS FOR THE FREEDERICKSZ CRITICAL FIELDS

In this section we report the finite size scaling analysis for the Freedericksz critical fields observed for slab thicknesses of $n_y = L = 10$, 20, 30, and 40 layers, respectively. The values of the critical fields $h_c(d)$ determined from the maximums of the apparent order parameters' S' and $C'/6$ susceptibilities are fitted with the values of $d = n_x = n_z = 6$, 8, 10, 12, 14, and

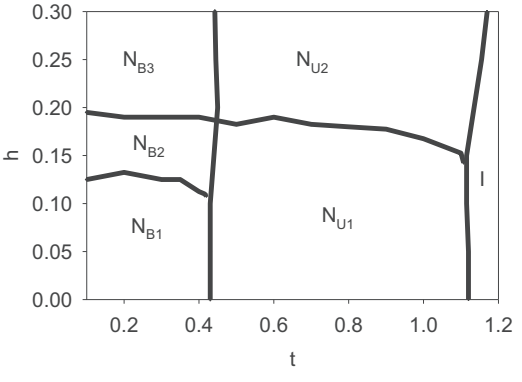

FIG. 16. System's phase diagram in the t-h plane. N_{B1}: undistorted biaxial nematic phase; N_{B2}: biaxial nematic with secondary director aligned with the field; N_{B3}: biaxial nematic with main director aligned with the field. N_{U1}: undistorted uniaxial nematic; N_{U2}: uniaxial nematic with director aligned with the field. I: isotropic phase.

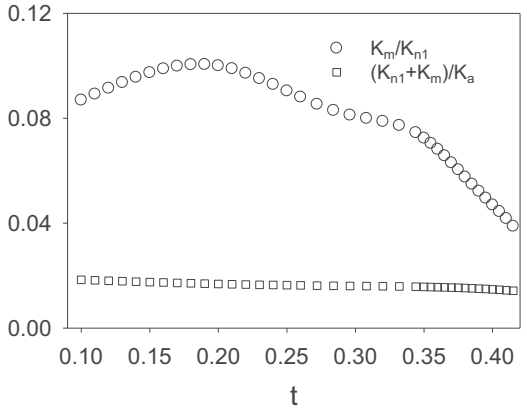

FIG. 17. Temperature dependence of the elastic constant ratios K_m/K_{n1} and $(K_{n1}+K_m)/K_a$, showing a sharp decrease of K_m as the N_B-N_U phase transition is approached.

16, using the following function:

$$\frac{1}{h_c(d)} = \frac{1}{h_c(d\to\infty)} - \frac{\text{const.}}{n_x}. \tag{12}$$

See Figs. 18–20 and Table I. Figure 20 shows that both $h_{cS}(\infty)$ and $h_{cC}(\infty)$ are both proportional to $n_y^{(-1)}$ as expected from continuum theory [25].

X. CRITICAL TEMPERATURES AND CRITICAL EXPONENTS

In this section we report on the critical behavior of the order parameters S and C, and the correlation lengths for the N_U-I and N_B-N_U phase transitions as determined from finite size scaling analysis using the data collapse method [28,29]. The analysis was carried out for $L = n_y$ ranging from 10 to 60 and for each n_y, the set of collapsed order parameter curves considered included $l = n_x = n_z$ ranging from 6 to 20. In the vicinity of the N_U-I transition which is continuous in our confined system it is possible to write $S \propto |t_r|^{\beta}$ and $\xi_S \propto |t_r|^{-\nu}$, where $t_r \equiv (t-t_c)/t_c$, ξ_S is the correlation length, t_c is the reduced critical temperature for the transition, and β and ν are critical exponents for the different quantities.

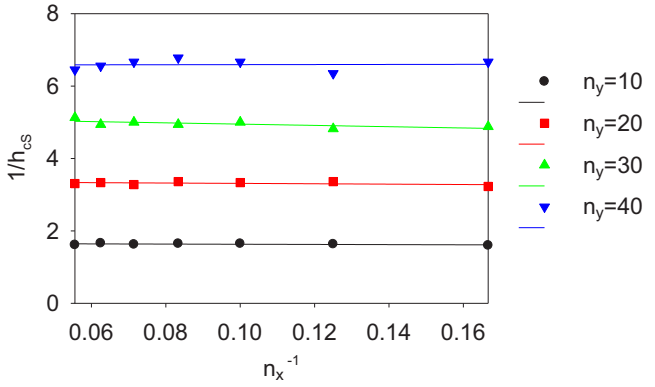

FIG. 18. $1/h_{cS}$ dependence on $1/n_x$ for the samples with different layers ($n_y = 10$ to 40) used in the scaling analysis of the Freedericksz critical fields for the main director reorientation.

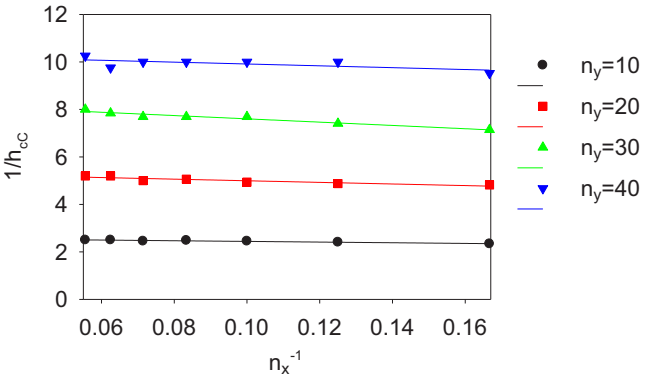

FIG. 19. $1/h_{cC}$ dependence on $1/n_x$ for the samples with different layers ($n_y = 10$ to 40) used in the scaling analysis of the Freedericksz critical fields for the secondary director reorientation.

Similar relations hold for C and ξ_c near the N_B-N_U transition with different values for T_c, β, and ν. Following Ref. [28] we consider a scaling function $\tilde{S}$ given by

$$\tilde{S}\left(l^{1/\nu}t_r\right) = l^{\beta/\nu}S(t_r),$$

which in accord with scaling analysis is independent of the system dimension $l = n_x = n_z$. Consequently, the different curves for $\tilde{S}$ obtained from the data sets with different l should coincide if T_c, β, and ν have the correct values for the transition. A similar calculation was carried out for the C order parameter at the N_B-N_U phase transition. The curves for S and the collapsed curves for $\tilde{S}$ are shown in Figs. 21 and 22. The critical temperature and the critical exponents' dependence on n_y for the order parameter S at the N_U-I phase transition are shown in Fig. 23; a plateau is approached as n_y goes above 30.

The curves for C and the collapsed curves for $\tilde{C}$ as a function of the reduced temperature are shown in Figs. 24 and 25. Figure 26 reports the reduced T_c, β, and ν dependencies on the system dimension l for the N_U-N_B transition. A plateau is approached as l increases.

The extrapolation of the values of the above critical exponents and critical temperature for S at the I-N transition

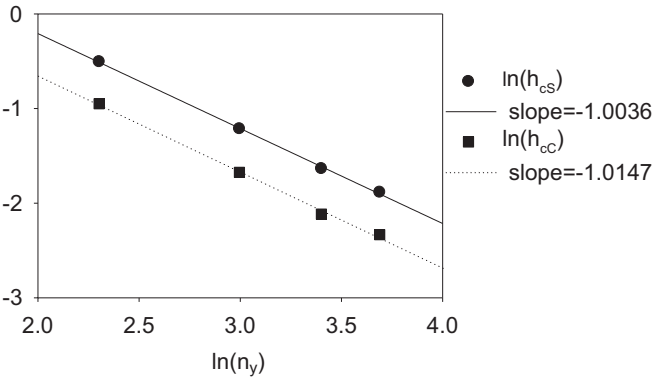

FIG. 20. Fit of $\ln[h_{c\infty}(n_y)]$ vs $\ln(n_y)$, $L = n_y = 10$, 20, 30, 40—circles: h_{cS}; squares: h_{cC}. Linear fit equations: S: 1.80–1.0036x; C: 1.3747–1.0147x. Thus $h_{c\infty}(n_y) \propto {n_y}^{-1}$, as expected from the continuum theory [25].

TABLE I. Fitting parameters $1/h_{cS}(\infty)$, const.$_S$, $1/h_{cC}(\infty)$, and const.$_C$ obtained by fitting Eq. (12) to the data shown in Figs. 18 and 19.

n_y	$1/h_{cS}(\infty)$	const.$_S$	$1/h_{cC}(\infty)$	const.$_C$
10	1.66 ± 0.02	0.3 ± 0.2	2.58 ± 0.02	1.4 ± 0.2
20	3.36 ± 0.05	0.5 ± 0.5	5.33 ± 0.07	3.4 ± 0.7
30	5.12 ± 0.08	1.8 ± 0.8	8.30 ± 0.08	6.9 ± 0.8
40	6.6 ± 0.2	0.1 ± 1.7	10.3 ± 0.2	3.9 ± 2.0

when $L \to \infty$ gives $\nu = 0.522 \pm 0.008$ $(0.512 \pm 9 \times 10^{-4})$, $\beta = 0.281 \pm 0.003$ $(0.278 \pm 3 \times 10^{-6})$, and $T_c = 1.1160 \pm 2 \times 10^{-7}$; the values parenthesized and T_c were obtained without the first point.

Using the following relations between the critical exponents [30],

Josephson: $(2-\alpha)/\nu d = 1$, where α is the heat capacity critical exponent and d the dimension,

Rushbrooke: $\alpha + 2\beta + \gamma = 2$, where γ is the order parameter susceptibility critical exponent,

and taking $d = 3$, gives $\alpha = 0.434\,(0.464)$, $\gamma = 1.004\,(0.982)$ that, together with the value(s) found for β, approach the values expected for a tricritical point [30]: $\alpha = 0.5$, $\beta = 0.25$, $\gamma = 1$, which could be indicating the proximity of a tricritical point.

Parameter *C*

The extrapolation of the values of the above critical exponents and critical temperature for C at the biaxial-uniaxial transition for $L \to \infty$ gives $\nu = 0.677 \pm 0.006$ $(0.672 \pm 9 \times 10^{-4})$, $\beta = 0.316 \pm 0.003$ $(0.313 \pm 8 \times 10^{-6})$, and $T_c = 0.4305 \pm 5 \times 10^{-8}$, the values parenthesized and T_c were obtained without the first point, as before.

Using the Josephson and the Rushbrooke relations between the critical exponents and taking $d = 3$, as for the parameter S, we find $\alpha = -0.031\,(-0.016)$, $\gamma = 1.398\,(1.390)$. These values suggest that this transition belongs to the 3D XY model universality class [31,32].

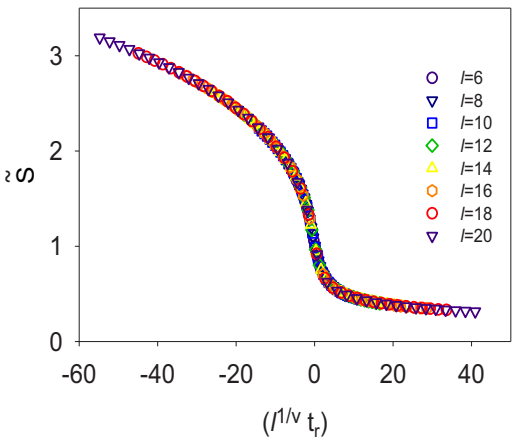

FIG. 22. $\tilde{S}$ scaling function curves as a function of $(l^{1/\nu}t_r)$ for eight different values of $l = n_x = n_z$ ranging from 6 to 20 and $n_y = 40$; the curves collapse can be observed.

XI. DISCUSSION AND CONCLUSIONS

The order parameters' t-h dependencies obtained show that the system exhibits five different configurations compatible with three distinct phases in the t-h range explored. The phases observed comprise an isotropic phase at higher temperatures, a uniaxial nematic at intermediate temperatures, and a biaxial nematic at the lowest temperatures. This is a particular case of the more general related system behavior studied in Refs. [19,20]. The electric field is seen to drive Freedericksz transitions in both the uniaxial and the biaxial nematics with the presence of two such transitions in the biaxial nematic, one occurring at the lower field associated with the reorientation of the secondary directors and the other occurring at higher field associated with the reorientation of the main director. The intrinsic order quantified by order parameters S and C seems largely unaffected by the electric field in the range explored. All the phase transitions observed either t driven or h driven

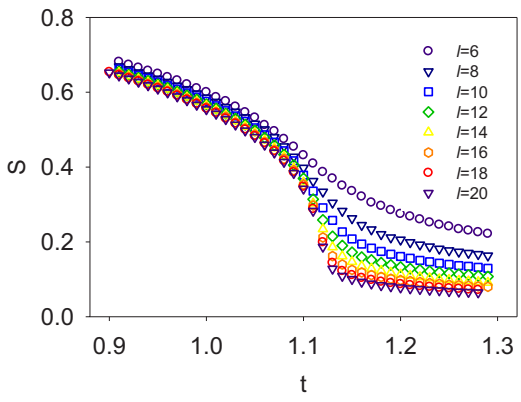

FIG. 21. Reduced temperature dependence of the order parameter S over the transition N_U-I for eight different values of the system size in the x and z directions, $l = n_x = n_z$ ranging from 6 to 20 and $n_y = 40$.

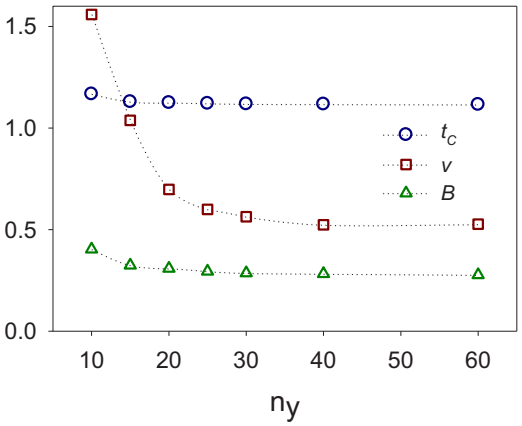

FIG. 23. Sample thickness $L = n_y$ dependence of the critical temperature T_c and the critical exponents ν and β for the order parameter S at the N_U-I phase transition. The dotted lines are guides to the eye.

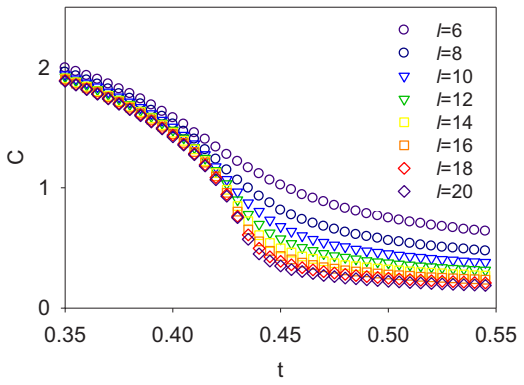

FIG. 24. Reduced temperature dependence of the order parameter C over the transition N_B-N_U for eight different values of the system size in the x and z directions; $l = n_x = n_z$ ranging from 6 to 20 and $n_y = 40$.

were found to be continuous, and while this was expected for the h driven transitions, for the order-disorder transition this is most probably a consequence of the confinement and limited size of the systems studied.

Regarding the system's field response, in the frame of the sample, the apparent uniaxial order parameter S' decreases weakly up to reduced fields $h \approx 0.02$ in the bulk, as the main director is strongly anchored to the wall and at the working temperature the uniaxial elastic constants are very strong. The marked decrease to negative values after the plateau indicates the onset of the Freedericksz transition of the main director. At stronger fields a saturation transition is expected, where $S \to -1/2$, i.e., **n** aligning with the field in the bulk of the sample [33]. A similar prediction was made using a Landau theory for molecules with cylindrical symmetry in a biaxial phase [34].

In the frame of the sample, the biaxial directors are strongly affected by the applied field in the bulk, as indicated by the behavior of the apparent order parameter C' taking negative values as the field increases (the faces of the molecules tend

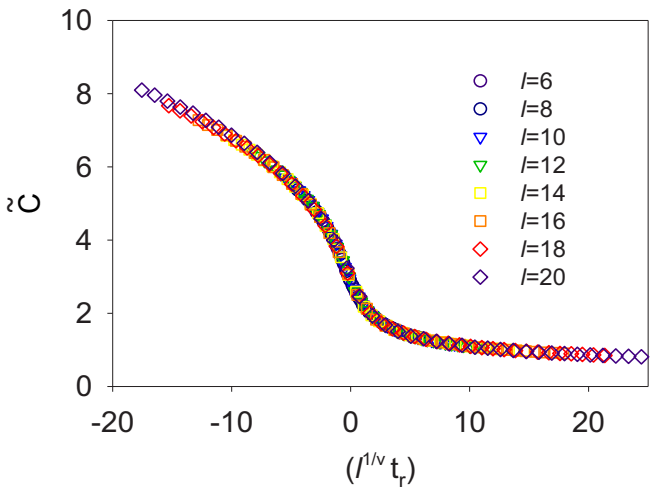

FIG. 25. $\tilde{C}$ scaling function curves as a function of $(l^{(1/\nu)}t_r)$ for seven different values of $l = n_x = n_z$ ranging from 6 to 20 and $n_y = 40$; the curve collapse can be observed.

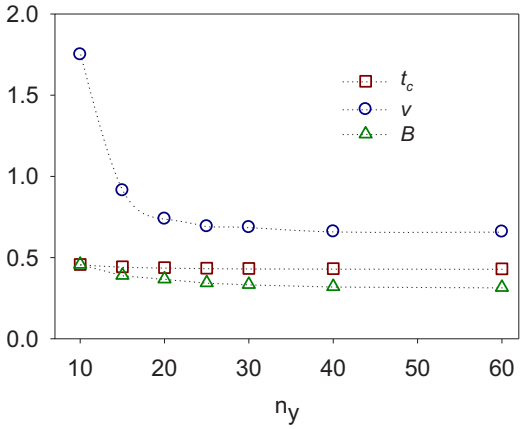

FIG. 26. Sample thickness $L = n_y$ dependence of the critical temperature T_c and the critical exponents ν and β for the order parameter C at the N_B-N_U phase transition. The dotted lines are guides to the eye.

to turn away from the surface, as sketched in Fig. 9). The Freedericksz transition of the secondary directors occurs at weaker field values than for the main director, due to the weaker values of the biaxial elastic constants. Interestingly, the curve of the C' parameter vs the field inverts its descent at the critical field for the S' parameter. Our simulations show that there is a metastable state where the S' plateau goes on for higher values of its critical field and, accordingly, the parameter C' continues its descent for the saturation transition (simulations not shown in this work).

The determined Freedericksz transition fields in the biaxial nematic phase allowed the calculation of two elastic constants ratios; one of them shows that the biaxial elastic constant decreases continuously on approaching the N_B-N_U phase transition and stays always below 11% of the main director splay constant. Finite size scaling analysis of the Freedericksz critical fields show that both Freedericksz transition fields in the biaxial phase scale with the inverse of the system thickness L in accord with continuum theory.

Finite size scaling analysis was used to obtain the critical temperature and critical exponents for the N-I transition and the N_B-N_U transition. Regarding the N-I transition, it is well known that the Lebwohl-Lasher model has a discontinuous isotropic-nematic transition in three dimensions [35] while in two dimensions it seems to exhibit a type of Berezinskii-Kosterlitz-Thouless–like transition [36,37]. In our case a biaxial extension of the Lebwohl-Lasher potential is used and the system is confined in one spatial direction with boundary surfaces inducing perfect order. The system thicknesses investigated ranging from 10 to 60 spin layers fall below the critical value for a discontinuous order-disorder transition to occur, leading to a continuous transition with the critical exponents β and ν for the relevant order parameter S for $L \to \infty$ (and α and γ using the Josephson and the Rushbrooke relations between critical exponents) pointing for the proximity of a tricritical point. The N_B-N_U transition is also continuous, and the results obtained for the critical exponents β and ν of the relevant order parameter C for $L \to \infty$ (and α and γ using the Josephson and the Rushbrooke relations as for S) suggest that this transition belongs to the 3D XY model

universality class [31,32]. This model in two dimensions (2D) exhibits a Berezinskii-Kosterlitz-Thouless–like transition, and in 3D is relevant to the critical behavior of a number of physical systems, such as magnetic and superfluid ^{4}He phase transitions; see [31], and references therein.

ACKNOWLEDGMENT

J.L.F. acknowledges financial support from the Portuguese Science and Technology Foundation (FCT) through CeFEMA Strategic Project No. UID/CTM/04540/2019.

[1] M. J. Freiser, Phys. Rev. Lett. **24**, 1041 (1970).
[2] R. Alben, Phys. Rev. Lett. **30**, 778 (1973).
[3] J. P. Straley, Phys. Rev. A **10**, 1881 (1974).
[4] G. R. Luckhurst, Thin Solid Films **393**, 40 (2001).
[5] L. J. Yu and A. Saupe, Phys. Rev. Lett. **45**, 1000 (1980).
[6] R. Hashim, G. R. Luckhurst, and S. Romano, Mol. Phys. **53**, 1535 (1984).
[7] M. P. Allen, Mol. Phys. **117**, 2391 (2019).
[8] S. D. Peroukidis, P. K. Karahaliou, A. G. Vanakaras, and D. J. Photinos, Liq. Cryst. **36**, 727 (2009).
[9] K. Trojanowski, D. W. Allender, L. Longa, and Ł. Kuśmierz, Mol. Cryst. Liq. Cryst. **540**, 59 (2011).
[10] E. F.Gramsbergen, L. Longa, and W. H. de Jeu, Phys. Rep. **135**, 195 (1986).
[11] R. Berardi, L. Muccioli, and C. Zannoni, J. Chem. Phys. **128**, 024905 (2008).
[12] S. Polineni, J. L. Figueirinhas, C. Cruz, D. A. Wilson, and G. H. Mehl, J. Chem. Phys. **138**, 124904 (2013).
[13] P. A. Lebwobl and G. Lasher, Phys. Rev. A **6**, 426 (1972).
[14] G. R. Luckhurst and S. Romano, Mol. Phys. **30**, 1345 (1975).
[15] X. Zheng and P. Palffy-Muhoray, Discrete Contin. Dyn. Syst., Ser. B **15**, 475 (2011).
[16] C. Chiccoli, P. Pasini, F. Semeria, and C. Zannoni, Int. J. Mod. Phys. C **10**, 469 (1999).
[17] F. Biscarini, C. Chiccoli, P. Pasini, F. Semeria, and C. Zannoni, Phys. Rev. Lett. **75**, 1803 (1995).
[18] N. Ghoshal, K. Mukhopadhyay, and S. K. Roy, Phys. Rev. E **89**, 042505 (2014).
[19] L. Longa, P. Grzybowski, S. Romano, and E. Virga, Phys. Rev. E **71**, 051714 (2005); **73**, 019904(E) (2006).
[20] G. De Matteis and S. Romano, Phys. Rev. E **78**, 021702 (2008).
[21] D. Dunmur and K. Toriyama, Tensor properties of anisotropic materials, in *Physical Properties of Liquid Crystals*, edited by D. Demus, J. Goodby, G. W. Gray, H.-W. Spiess, and V. Vill (Wiley-VCH Verlag GmBH, Weinheim, Germany, 1999), pp. 87–101.
[22] H. Goldstein, C. Poole, and J. Safko, *Classical Mechanics*, 3rd ed. (Addison-Wesley, Boston, 2001).
[23] D. P. Landau and K. Binder, *A Guide to Monte Carlo Simulations in Statistical Physics*, 3rd ed. (Cambridge University Press, Cambridge, 2010).
[24] R. Berardi, L. Muccioli, S. Orlandi, M. Ricci, and Claudio Zannoni, J. Phys.: Condens. Matter **20**, 463101 (2008).
[25] P. G. de Gennes and J. Prost, *The Physics of Liquid Crystals* (Oxford University Press, Oxford, 1993).
[26] H.-R. Trebin, J. Phys. (France) **42**, 1573 (1981).
[27] D. Dunmur and K. Toriyama, Dielectric properties, in *Physical Properties of Liquid Crystals* (Wiley-VCH Verlag GmBH, Weinheim, Germany, 1999), p. 129.
[28] M. E. J. Newman and G. T. Barkema, *Monte Carlo Methods in Statistical Physics* (Oxford University Press, Oxford, 1999), Chap. 8, p. 232.
[29] K. Binder and D. W. Heermann, *Monte Carlo Simulation in Statistical Physics* (Springer, Berlin, Heidelberg, 2010), Chap. 4, p. 77.
[30] K. Huang, *Statistical Mechanics*, 2nd ed. (John Wiley & Sons, New York, 1987).
[31] A. P. Gottlob and M. Hasenbusch Phys. A (Amsterdam, Neth.) **201**, 593 (1993).
[32] M. Campostrini, M. Hasenbusch, A. Pelissetto, P. Rossi, and E. Vicari, Phys. Rev. B **63**, 214503 (2001).
[33] C. Chiccoli, S. Guzzetti, P. Pasini, and C. Zannoni, Mol. Cryst. Liq. Cryst. **360**, 119 (2001).
[34] M. Kio, M. Torikai, and M. Yamashita, Opto-Electron. Rev. **17**, 8 (2009).
[35] G. R. Luckhurst and P. Simpson, Mol. Phys. **47**, 251 (1982).
[36] R. Paredes V., A. I. Farinas-Sánchez, and R. Botet, Phys. Rev. E **78**, 051706 (2008).
[37] N. G. Almarza, C. Martín, and E. Lomba, Phys. Rev. E **82**, 011140 (2010).